NASA Technical Memorandum 102582

PERSONAL COMPUTER STUDY OF FINITE-DIFFERENCE METHODS FOR THE TRANSONIC SMALL DISTURBANCE EQUATION

SAMUEL R. BLAND

DECEMBER 1989

National Aeronautics and Space Administration

Langley Research Center
Hampton, Virginia 23665-5225

PERSONAL COMPUTER STUDY OF FINITE-DIFFERENCE METHODS FOR THE TRANSONIC SMALL DISTURBANCE EQUATION

Samuel R. Bland

NASA Langley Research Center, USA

ABSTRACT

Calculation of unsteady flow phenomena requires careful attention to the numerical treatment of the governing partial differential equations. The personal computer provides a convenient and useful tool for the development of meshes, algorithms, and boundary conditions needed to provide time accurate solution of these equations. The one-dimensional equation considered in this paper provides a suitable model for the study of wave propagation in the equations of transonic small disturbance potential flow. Numerical results for effects of mesh size, extent, and stretching, time step size, and choice of far-field boundary conditions are presented. Analysis of the discretized model problem supports these numerical results. Guidelines for suitable mesh and time step choices are given.

1–INTRODUCTION

At present, transonic small disturbance (TSD) potential theory provides the only practical method for the aeroelastic analysis of complete aircraft configurations at transonic speeds (Batina et al. [1]). In order to compute a time accurate flow field, careful attention must be given to the mesh design and boundary conditions. Mesh fineness, extent, and stretching all affect the accuracy with which the wave-like disturbances inherent in the unsteady flow field can be described.

In applications of an early TSD code (Whitlow [2]), problems associated with poor mesh design were encountered in calculating the unsteady lift and moment on an oscillating airfoil. The nature of the inaccuracies is illustrated in figure 1 (Seidel [3]). Shown are the real and imaginary parts of the lift curve slope for a flat-plate airfoil as functions of pitching frequency, compared with the exact linear theory results (Bland [4]) with which they should agree. Figure 1(a) shows results calculated using an exponentially stretched mesh which extends several hundred chord-lengths from the airfoil.

Figure 1(b) shows the improvement obtained with a better mesh design (25 chord-length extent) and proper choice of the far-field boundary conditions.

These and other difficulties associated with time-marching finite-difference methods in TSD may be studied using much simplified model equations on a personal computer. The use of the BASIC computer language with real-time graphics provides insight into difficulties arising from both the discretization of the continuous process being modeled and the solution algorithm used. Such insights are much more expensive and time consuming to obtain from solutions of the complete equations on a supercomputer. With the sole exception of figure 1, the figures in the present paper were produced from copies of the personal computer screen on a dot matrix printer.

The one-dimensional linear wave equation provides a model for the propagation of signals in the vertical direction, which are an important component of solutions of the unsteady TSD equation. Finite-difference solutions of this linear second-order partial differential equation illustrate the care needed to capture the wave propagation in the unsteady potential flow problem. Furthermore, the one-dimensional finite-difference equation is subject to analytical treatment (Vichnevetsky [5]), which sheds additional light on the numerical results. The importance of mesh fineness, extent, and stretching and the proper treatment of both near- and far-field boundary conditions are demonstrated in this paper.

2–ANALYSIS AND RESULTS

The transonic small disturbance equation in its simplest form may be written as

$$(1 - M^2 - (\gamma + 1)M^2\phi_x)\phi_{xx} + \phi_{zz} = 2M^2\phi_{xt} + M^2\phi_{tt} \tag{1}$$

for two-dimensional flow. Elementary solutions of this equation for linear subsonic flow represent circular waves radiating outward as their centers are convected downstream. Waves propagating along a particular direction may be investigated by considering one-dimensional wave motion. In particular the difficulties encountered in the TSD results of figure 1 have been identified with wave reflections in the vertical direction.

2.1–One-dimensional wave equation

The effects of mesh extent, spacing, and stretching on the solution of the TSD flow equation are clearly shown in the study of the wave equation

$$\phi_{tt} = c^2\phi_{zz} \tag{2}$$

This equation is obtained from equation (1) by omitting the x-derivative terms and recognizing that M plays the role of the reciprocal of the wave propagation speed c in the nondimensional coordinates used.

The usefullness of this approach in understanding problems encountered in TSD calculations is demonstrated in figure 2. Numerical solutions are given for the response to a pulse in ϕ_z (analogous to the pulse in angle of attack used to generate the TSD results of figure 1). In each case the finite-difference potential $\varphi(0,t)$ at $z = 0$, is given as a function of time in the left part of the figure. The resulting frequency response functions $F(k)$ are plotted on the right. Figures 1a and 2a use the same exponentially

stretched mesh in the z-direction. The quadratically stretched mesh of 25 chord-lengths extent proposed by Seidel [3] is used in figures 1b and 2b-c. Figure 2c shows the effect of using an improper far-field boundary-condition. The results of figure 2 are remarkably similar to those shown in figures 1–2 of Edwards [6] for the TSD equation. In particular, the oscillations in the time history $\varphi(0,t)$ in figure 2a are known to originate from the large mesh stretching used and typically lead to oscillations in the frequency response function $F(k)$ similar to those seen in this figure. Furthermore, the disturbance in the time history at $t \approx 50$ in figure 2c originates from a far-field boundary reflection and leads to the oscillations seen in $F(k)$ at low values of k.

The wave equation (2) has a general solution of the form

$$\phi(z,t) = F(z - ct) + G(z + ct) \tag{3}$$

in which F and G represent waves propagating in the positive ($z - ct$ constant) and negative ($z + ct$ constant) z-directions with speed c.

To simulate the vertical component of the fluid flow problem, we may solve this problem in the quarter plane $z, t \geq 0$ subject to two initial conditions at $t = 0$ and boundary conditions at $z = 0$ and ∞. To solve our model problem numerically, we must discretize the continuous variables z, t and replace the partial derivatives in equation (2) by finite-difference analogues. Finally, the boundary condition at $z = \infty$ must be replaced by a condition at some finite value $z = L$.

Before proceeding with the details of the numerical approach, several illustrations of the nature of the difficulties with numerical solutions of an initial value problem will be given. Calculations for an initial wave packet at $t = 0$ are shown in figures 3. Exponentially stretched meshes of varying fineness (illustrated beneath each figure) are used and the solutions are given at every other time step using a small step size. In figure 3(a) the wave propagating outwards encounters a reflecting boundary at the right and a non-reflecting boundary at the left. The initial pulse divides into two pulses which propagate outward with little distortion until the boundary is encountered. In figure 3(b) the same 97-point mesh is used with non-reflecting boundary conditions at both sides. Figure 3(c) is for a coarser mesh which allows significant reflection from the boundaries to occur. In figure 3(d) the mesh has become so coarse that essentially all of the wave is reflected from within the mesh, even before reaching the boundaries. For this case, at the boundaries there are only about two mesh points per wave length. Most of the wave energy is trapped within the mesh. In an aerodynamic problem, the wing would remain near $z = 0$ and would encounter these non-physical mesh reflections. The initial pulse contains components of all frequencies and, as we shall see, the higher frequencies propagate more slowly and therefore lag behind the main (low frequency) wave.

The initial conditions for the remainder of the paper will be

$$\phi(z,0) = 0 \quad \text{and} \quad \phi_t(z,0) = 0 \tag{4}$$

As the boundary condition at $z = 0$ we use

$$\phi_z(0,t) = f(t) \tag{5}$$

This condition is analogous to imposing a condition on the vertical velocity (downwash) at the oscillating airfoil surface in the aerodynamics problem. Finally, we must impose a boundary condition at $z = L$ which simulates the outgoing wave condition at infinity in the original problem. The proper choice for this wave propagating upward is

$$\phi_t(L,t) + c\phi_z(L,t) = 0 \tag{6}$$

2.2–Finite-difference formulation

The one-dimensional model equation (2) is discretized in a manner identical to that used for the vertical z and time t coordinates of the TSD equation in the program described by Batina [7]. The second-order accurate backward difference approximation for the t-derivative at the new time level $n+1$ is

$$\partial_{tt}\varphi = (2\varphi^{n+1} - 5\varphi^n + 4\varphi^{n-1} - \varphi^{n-2})/\Delta t^2 \tag{7}$$

which involves four time levels. For reference we also state the first-order accurate form

$$\partial_{tt}\varphi = (\varphi^{n+1} - 2\varphi^n + \varphi^{n-1})/\Delta t^2 \tag{8}$$

The second-order accurate central difference approximation for the z-derivative is

$$\partial_{zz}\varphi = \frac{2}{z_{j+1} - z_{j-1}} \left(\frac{\varphi_{j+1} - \varphi_j}{z_{j+1} - z_j} - \frac{\varphi_j - \varphi_{j-1}}{z_j - z_{j-1}} \right) \tag{9}$$

in which this equation applies at the internal mesh points $0 < j < J$.

The boundary condition in equation (5) at $z = 0$ may be incorporated by solving the differential equation (2) at z_0 using

$$\partial_{zz}\varphi = \frac{2}{z_0 + z_1} \left(\frac{\varphi_1 - \varphi_0}{z_1 - z_0} - f(t) \right) \tag{10}$$

in which the zeroth mesh point z_0 need be only near $z = 0$.

The far-field condition in equation (6) is derived by applying the boundary condition at $j = J - 1/2$. The second-order accurate formulas needed are

$$\partial_z\varphi = \frac{\varphi_J - \varphi_{J-1}}{z_J - z_{J-1}} \tag{11}$$

and

$$\partial_t\varphi = (3\varphi^{n+1} - 4\varphi^n + \varphi^{n-1})/2\Delta t \tag{12}$$

and the first-order accurate formula is

$$\partial_t\varphi = (\varphi^{n+1} - \varphi^n)/\Delta t \tag{13}$$

The t-derivatives in equations (12) and (13) are evaluated at $j = J - 1/2$ by applying the operations on the right hand sides to the average $(\varphi_{J-1} + \varphi_J)/2$.

2.3–Model equation

There is no loss of generality in normalizing the time t such that the wave speed becomes $c = 1$. This choice slightly simplifies the analysis.

Continuous Problem To be specific, in the quarter-plane $t, z \geq 0$, solve

$$\phi_{tt} = \phi_{zz} \qquad \text{for } t, z > 0 \tag{14a}$$

$$\phi(z,0) = \phi_t(z,0) = 0 \qquad \text{for initial conditions} \tag{14b}$$

$$\phi_z(0,t) = f(t) = -\omega \sin \omega t \qquad \text{for downwash b.c.} \tag{14c}$$

$$\phi_t + \phi_z = 0 \quad \text{as } z \to \infty \qquad \text{for outgoing wave} \tag{14d}$$

The exact solution is

$$\phi(z,t) = 1 - \cos \omega(t - z) \qquad \text{for } z < t \tag{15}$$

and 0 otherwise. This solution represents an undistorted wave propagating upward with unit speed $c = 1$. We remark that this solution satisfies the outgoing wave condition of equation (14d) everywhere.

Semi-Discrete Problem The semi-discrete analysis ('method of lines') considers the effect of the spatial discretization only, while treating the time as continuous. The mesh characteristics are thereby isolated from the questions associated with time step size (i.e., Courant number ν) such as stability.

For a uniform mesh

$$z_j = hj \qquad \text{for } j = 0, 1, \ldots, J \tag{16}$$

with constant spacing $h = \Delta z$, central differencing provides $O(h^2)$ accuracy. Letting $\dot{\varphi} = \partial\varphi/\partial t$, the semi-discrete version of equation (14) is

$$\ddot{\varphi}_0 = (2/h^2)(\varphi_1 - \varphi_0) + (2\omega/h) \sin \omega t \tag{17a}$$

$$\ddot{\varphi}_j = (1/h^2)(\varphi_{j-1} - 2\varphi_j + \varphi_{j+1}) \tag{17b}$$

$$\dot{\varphi}_{J-1} + \dot{\varphi}_J = (2/h)(\varphi_{J-1} - \varphi_J) \tag{17c}$$

Vichnevetsky and Bowles [8] and Vichnevetsky [5, 9], provide an extensive treatment of the problems encountered in using finite-difference methods to solve equations governing wave-like phenomena. They concentrate on the first order advection equation (a model for the Euler equations) rather than the wave equation treated herein. Trefethen [10] gives the analysis and some numerical results for both the one- and two-dimensional equations. For the analysis, we assume that the solution is harmonic in time and space and determine the conditions implied by this assumption. For more complicated wave-forms the ideas of Fourier analysis apply. This approach does not capture the transient effects present in the initial value problem, but looks at the steady-state behavior.

Substitution of the harmonic trial solution

$$\varphi_j(t) = e^{i(\omega t - \xi z_j)} \tag{18}$$

into equation (17b) yields the dispersion relation. Dispersion refers to the fact that waves with different frequencies will propagate at different speeds. We obtain

$$\sin\frac{\xi h}{2} = \pm\frac{\omega h}{2} \tag{19}$$

in which we consider the temporal frequency ω as given and the spatial wave number ξ as unknown. Choosing the $+$ sign for the upward propagating wave yields

$$\xi = \frac{2}{h}\arcsin\frac{\omega h}{2} \sim \omega\left(1+\frac{1}{6}\left(\frac{\omega h}{2}\right)^2\right) > \omega \tag{20}$$

Note that as $\omega h \to 0$, we recover, as expected, the exact solution for which $\xi = \omega$.

If we restrict attention to the outgoing wave solution (semi-infinite mesh extent), the $+$ sign in equation (19) is selected and imposing the boundary condition equation (17a) then yields the exact solution for the semi-discrete problem

$$\varphi_j(t) = 1 - \frac{1}{\sqrt{1-(\omega h/2)^2}}\cos(\omega t - \xi z_j) \tag{21}$$

which is also an exact solution of the 'continuous' problem

$$\varphi_{tt} = c^{*2}\varphi_{zz} \tag{22}$$

in which the phase velocity

$$c^* = \frac{\omega}{\xi} = \frac{\omega h/2}{\arcsin\omega h/2} \sim 1 - \frac{1}{6}\left(\frac{\omega h}{2}\right)^2 < 1 \tag{23}$$

replaces the original wave speed $c = 1$, provided that we identify the discrete variable z_j with the continuous variable z.

These results provide a great deal of insight into the behavior of the numerical solution. Note that it depends only on c^*, a function of ωh, so that increasing either ω or h has the same effect. Equation (19) implies $|\omega h/2| \leq 1$ (cut-off frequency) in order for harmonic solutions to exist, although other types of behavior may appear (Vichnevetsky [5, 9]). The wave propagates with the phase velocity c^* and wave length

$$\lambda^* = 2\pi/\xi = c^*\lambda < \lambda \tag{24}$$

where $\omega < \xi \leq \pi/h$ so that the numerical wave propagates more slowly than the exact wave and has a shorter length. The amplitude is too large by the factor

$$A = \frac{1}{\sqrt{1-(\omega h/2)^2}} \sim 1 + \frac{1}{2}\left(\frac{\omega h}{2}\right)^2 \tag{25}$$

The decreasing propagation speed c^* with increasing mesh spacing h lies at the root of the strange behavior of the solution on the stretched meshes illustrated in figure 3.

The analysis shows that these effects are present in the semi-discrete equation and do not depend on the time step used.

The decrease in propagation speed (equation (23)) and increase in amplitude (equation (25)) for a harmonic wave are clearly seen in figure 4. In figure 4(a) the solution $\varphi(z,t)$ on a uniform 49-point mesh is shown at $t = 16$. The numerical wave is propagating more slowly across the mesh than the exact wave. In figure 4(b) the solution time history $\varphi(0,t)$ is shown. For the parameters used here, $\omega = \pi$, $h = 1/3$, we expect $c^* = 0.95$ and $A = 1.17$. The numerical results agree with these values. For this example there are six mesh points per spatial wave length, which is a reasonable minimum number to capture the propagating signal.

The analysis considered to this point correctly describes the behavior of the numerical solution of the semi-discrete equation on a semi-infinite mesh as $t \to \infty$. Considering now the effect of limited mesh extent, we will show that the second-order accurate non-reflecting far-field boundary condition equation (17c) produces a partial reflection of the outward propagating wave. For an incident wave, equation (21) with amplitude A

$$\varphi^i = 1 - A\cos(\omega t - \xi z) \tag{26}$$

the reflected wave is

$$\varphi^r = -A\frac{A-1}{A+1}\cos\left(\omega t + \xi(z - 2L)\right) \tag{27}$$

where $L = (z_{J-1} + z_J)/2$ is the numerical boundary location. This reflected wave has an amplitude reduced from that of the incident wave by the reflection ratio

$$\rho = \frac{A-1}{A+1} \sim \frac{1}{4}\left(\frac{\omega h}{2}\right)^2 \tag{28}$$

and is propagating in the negative z-direction from an image point located two mesh extents from the origin. It is difficult to observe such reflections for the harmonic boundary condition under discussion here. However, they will be seen in the results for the pulse boundary condition given below.

The semi-discrete harmonic analysis may also be used to show that changes in mesh spacing produce internal (as opposed to boundary) reflections. This analysis has application to the results observed on stretched meshes. Consider a mesh with a single change in spacing at $z = 0$. Let the spacing be h for $z < 0$ and H for $z > 0$ with corresponding wave numbers ξ_h and ξ_H. We wish to determine the reflection that occurs when the upward propagating wave of unit amplitude passes through the discontinuity. We remark that the change in ξ at the interface leads to a change in the phase velocity c^* there. Away from the interface the solutions will be

$$\varphi_j(t) = e^{i(\omega t - \xi_h z_j)} + \rho e^{i(\omega t + \xi_h z_j)} \tag{29}$$

for $z_j < 0$ and

$$\varphi_j(t) = \tau e^{i(\omega t - \xi_H z_j)} \tag{30}$$

for $z_j > 0$. Here ρ is the reflection ratio and τ is the transmission ratio. These parameters are determined by applying equation (9) at the interface point z_j yielding

$$\ddot{\varphi}_j = \frac{2}{H+h}\left(\frac{\varphi_{j+1}-\varphi_j}{H} - \frac{\varphi_j - \varphi_{j-1}}{h}\right) \tag{31}$$

and by enforcing continuity to give a second equation

$$\tau = 1 + \rho \tag{32}$$

The solution is a little complicated and it suffices to show the asymptotic results for small mesh spacings and/or frequency

$$\rho \sim \left(\frac{\omega}{4}\right)^2 (H^2 - h^2) \tag{32}$$

$$\tau \sim 1 + \left(\frac{\omega}{4}\right)^2 (H^2 - h^2) \tag{33}$$

Note that as the wave passes through an interface with increased mesh spacing ($H > h$), the amplitude of the transmitted wave is increased. This result suggests that the amplitude would continue to grow as a wave propagates through a stretched mesh like those normally used in solving exterior flow problems.

These reflections are illustrated in figure 5 for a pulse in $\varphi_z(0,t)$. The pulse is centered at $t_c \approx 2$ and the mesh has spacings $h = 3/8$ for $0 < z < 6$ and $H = 3/4$ for $6 < z < 12$ ('bi-uniform mesh'). In figure 5(a) the exact and numerical waves are shown at $t = 6$. The solutions at the boundary $\varphi(0,t)$ are shown in figure 5(b). The bold tic-marks indicate the times for the center of the pulse and its reflection from the far-field to occur. Three different effects may be noted: (1) the return of the boundary reflection at $t \approx 26$; (2) the reflection generated by the mesh discontinuity at $t \approx 14$; (3) the oscillations near $t \approx 3$ which are caused by too large a spacing to accurately define the pulse boundary condition imposed at $z = 0$. In figure 5(c) the effects of these inaccuracies on the frequency response function are shown. From the view point of the aeroelastician, the results might be satisfactory since little error occurs for $k < 0.3$.

Additional insight into the behavior of the solution of the semi-discrete equation (31) on stretched meshes may be obtained by examining the modified equation (Anderson et al. [11]). This equation is obtained by Taylor series expansion of the potentials. For the uniform mesh the modified equation contains only even derivative terms and has constant coefficients. For the nonuniform mesh, derivatives of all orders are present and, in general, the coefficients are functions of z. A unique feature of the quadratically stretched mesh proposed by Seidel [3] is that the coefficient of the third derivative term in the modified equation is a small constant.

Fully Discrete Problem For simplicity, the analysis of the fully discrete equations will be given only for the case of the uniform mesh. As in Batina [7], the time differencing is written in implicit form. Both the first- and second-order time accurate equations will be displayed, then the dispersion relations will be given and the implications for the numerical solutions will be addressed.

The equations of $O(\Delta t)$, obtained from equations (8), (13), and (17) are

$$(1+2\nu^2)\varphi_0^{n+1} - 2\nu^2\varphi_1^{n+1} = 2\varphi_0^n - \varphi_0^{n-1} - 2h\nu^2 f(t) \tag{34a}$$

$$-\nu^2\varphi_{j-1}^{n+1} + (1+2\nu^2)\varphi_j^{n+1} - \nu^2\varphi_{j+1}^{n+1} = 2\varphi_j^n - \varphi_j^{n-1} \tag{34b}$$

$$(1-2\nu)\varphi_{J-1}^{n+1} + (1+2\nu)\varphi_J^{n+1} = \varphi_{J-1}^n + \varphi_J^n \tag{34c}$$

in which equation (34b) applies for $0 < j < J$.

The equations of $O(\Delta t^2)$, obtained from equations (7), (12), and (17) are

$$2(1+\nu^2)\varphi_0^{n+1} - 2\nu^2\varphi_1^{n+1} = 5\varphi_0^n - 4\varphi_0^{n-1} + \varphi_0^{n-2} - 2h\nu^2 f(t) \tag{35a}$$

$$-\nu^2\varphi_{j-1}^{n+1} + 2(1+\nu^2)\varphi_j^{n+1} - \nu^2\varphi_{j+1}^{n+1} = 5\varphi_j^n - 4\varphi_j^{n-1} + \varphi_j^{n-2} \tag{35b}$$

$$(3-4\nu)\varphi_{J-1}^{n+1} + (3+4\nu)\varphi_J^{n+1} = 4(\varphi_{J-1}^n + \varphi_J^n) - (\varphi_{J-1}^{n-1} + \varphi_J^{n-1}) \tag{35c}$$

in which equation (35b) applies for $0 < j < J$.

The tridiagonal systems in equations (34) and (35), which include the boundary conditions, may be solved using the Thomas algorithm (Anderson et al. [11], p.128). These equations have been used for all of the numerical results presented herein.

The dispersion relations are obtained by substituting the harmonic trial solution

$$\varphi_j^n = e^{i(\omega t_n - \xi z_j)} \tag{36}$$

with $z_j = j\Delta z$ and $t_n = n\Delta t$ into the field equations and dividing by φ_j^n. The result for the $O(\Delta t)$ equation (34b) is

$$\frac{1}{\Delta z}\sin\frac{\xi\Delta z}{2} = \frac{1}{\Delta t}e^{-i\omega\Delta t/2}\sin\frac{\omega\Delta t}{2} \tag{37}$$

It suffices to give the asymptotic solution of this equation which is

$$\xi \sim \omega\left(1 + \frac{\omega^2}{24}(\Delta z^2 - 4\Delta t^2) - i\frac{\omega}{2}\Delta t + O(\omega^3\Delta^3)\right) \tag{38}$$

The result for the $O(\Delta t^2)$ equation (35b) is

$$\frac{1}{\Delta z}\sin\frac{\xi\Delta z}{2} = \frac{1}{\Delta t}e^{-i\omega\Delta t/2}\sin\frac{\omega\Delta t}{2}\sqrt{2 - e^{-i\omega\Delta t}} \tag{39}$$

for which

$$\xi \sim \omega\left(1 + \frac{\omega^2}{24}(\Delta z^2 + 11\Delta t^2) - i\frac{7\omega^3}{16}\Delta t^3 + O(\omega^4\Delta^4)\right) \tag{40}$$

In both equations (38) and (40) the negative imaginary parts lead to an exponential decay of the solution with increasing z. In particular the amplitudes decay as $e^{-\omega^2\Delta t z/2}$ for the $O(\Delta t)$ equation and as $e^{-7\omega^4\Delta t^3 z/16}$ for the $O(\Delta t^2)$ equation. Thus, in contrast with the result for the semi-discrete analysis, which predicts that the propagating harmonic wave will have its amplitude increased (see equation (25)), the effect of the time discretization is to produce both a spreading out of the frequencies and a decrease in amplitude with increasing distance z from the source of the disturbance

at the origin. Also, we see that the first-order method is much more dissipative than the second-order one. This greater dissipation makes the first-order method much more forgiving of poor mesh design and choice of far-field boundary conditions, at least in applications to problems for which only the near-field solution is of interest.

The wave propagation speeds are computed from the real parts of the dispersion relations (equations (38) and (40)). For the two cases under consideration here, we see that the phase velocities will be approximately

$$c^* = \mathrm{Re}\{\omega/\xi\} \sim 1 - \frac{\omega^2}{24}(\Delta z^2 - 4\Delta t^2) \tag{41}$$

for the $O(\Delta t)$ equation (38) and

$$c^* = \mathrm{Re}\{\omega/\xi\} \sim 1 - \frac{\omega^2}{24}(\Delta z^2 + 11\Delta t^2) \tag{42}$$

for the $O(\Delta t^2)$ equation (40). Note that in equation (41) the error will vanish for $\nu = \Delta t/\Delta z = 1/2$, while no such possibility holds for the $O(\Delta t^2)$ equation.

In order to treat a nonuniform mesh using the uniform mesh results we may apply the conclusions just reached in a local sense (Vichnevetsky [9]). Then, for example, as a wave propagates into a stretching mesh we would expect both the dispersion (separation of frequencies) and dissipation (amplitude decay) to increase as the local Δz increases. One can think of the harmonic solution given above as remaining approximately valid by simply treating Δz as a function of z. An alternative approach is to consider perturbation solutions of the nonconstant coefficient modified equation.

The effects of time step size and order of accuracy are illustrated in the final four figures. In order to reduce the appearance of far-field boundary reflections, a mesh is used which stretches quadratically from both boundaries. The mesh contains 25 points and extends to $z = 8$. The mesh spacing varies from $\Delta z = 0.03$ at the ends to 0.64 in the center. The time step sizes are $\Delta t \approx 1/8$ and $1/2$. The calculations are carried to a total time of about 64 to allow all transients and reflections to die out.

Figures 6–7 give results using the second-order accurate equation (35). For the larger time step in figure 6, the solution spreads out as it propagates across the mesh (figure 6(a)). No reflections are apparent in the time history shown in figure 6(b). Although the frequency response results (figure 6(c)) are smooth, large errors are present for $k > 0.5$ which would go un-noted were the exact results not available for comparison. For the smaller time step results of figure 7, an unanticipated difficulty appears in the many high frequency oscillations in the time history of figure 7(b). These oscillations are also seen in the trailing part of the spatial wave in figure 7(a). In a TSD calculation, the appearance of oscillations like these in a solution might lead to nonlinear instability. However, the frequency response results of figure 7(c) are quite good for $k < 1$.

Figures 8–9 give results using the first-order accurate equation (34). Here the results are quite smooth for both time step sizes and no inaccuracies are apparent in the frequency response results of either figure 8(c) or 9(c), although large errors occur for the larger time step (figure 8). Examination of figure 8(b) shows that the numerical result predicts that the pulse center occurs too early in time. An arbitrary shift of

$\Delta t/2$ in the application of the forcing function $f(t)$ in equation (34a) corrects this discrepancy very nicely.

In choosing a vertical mesh for use in solving the TSD equation, one would not in general be able to 'waste' mesh points at the far-field boundaries by employing the very small spacing used in these examples, especially in three-dimensions. Nevertheless, the spacing must not be allowed to grow too large in the mid-field and should reduce somewhat at the far-field boundaries in order to avoid the appearance of non-physical oscillations in the calculation.

3–CONCLUSIONS

The personal computer provides a convenient and useful tool for the study of the techniques of mesh and algorithm design needed to provide time accurate solutions of the unsteady flow equations. The one-dimensional wave equation considered in this paper provides a suitable model equation for studying wave propagation in the vertical direction in transonic small disturbance potential flow. The following conclusions may be drawn from this study:

(1) The appearance of non-physical oscillations in the solution may result from either (a) inappropriate use of reflecting boundary conditions, (b) too large a mesh spacing at the boundary to correctly model the boundary condition, or (c) too much stretching of the mesh, leading to internal reflections.

(2) In order to accurately convect wave like disturbances through the finite-difference mesh, there must be at least six mesh points per spatial wave length.

(3) First-order time accurate methods are much more forgiving of poor mesh design than are second-order methods. The higher dissipation present with the first-order methods reduces the appearance of unwanted reflections, but at the price of a much poorer simulation of the overall flow field.

(4) Improved finite-difference meshes may be designed using the one-dimensional model problem as a guide.

4–NOMENCLATURE

A	amplitude of wave
c	wave speed in exact solution
c^*	phase velocity in discrete solution
$F(k)$	frequency response function
$f(t)$	boundary value of ϕ_z
J	index of last mesh point
j	index for discrete z
k	reduced frequency
L	far-field boundary for z
M	Mach number
n	index for discrete t
t	time
x	streamwise coordinate
z	vertical coordinate

λ	spatial wave length in exact solution
λ^*	spatial wave length in discrete solution
ν	Courant number $c\Delta t/\Delta z$
ξ	wave number
ρ	wave reflection ratio
τ	wave transmission ratio
ϕ	continuous perturbation potential
φ	discrete perturbation potential

5–REFERENCES

1. Batina, John T., Seidel David A., Bland, Samuel R., and Bennett, Robert M., Unsteady Transonic Flow Calculations for Realistic Aircraft Configurations, *Journal of Aircraft*, vol. 26, no. 1, pp. 21–28, 1989.
2. Whitlow, Woodrow, Jr., XTRAN2L: A Program for Solving the General-Frequency Unsteady Transonic Small Disturbance Equation, NASA TM 85723, November 1983.
3. Seidel, David A., Bennett, Robert M., and Whitlow, Woodrow, Jr., An Exploratory Study of Finite Difference Grids for Transonic Unsteady Aerodynamics, NASA TM 84583, December 1982.
4. Bland, Samuel R., Development of Low-Frequency Kernel-Function Aerodynamics for Comparison with Time-Dependent Finite-Difference Methods, NASA TM 83283, May 1982.
5. Vichnevetsky, Robert, Wave Propagation Analysis of Difference Schemes for Hyperbolic Equations: A Review, *International Journal for Numerical Methods in Fluids*, vol. 7, pp. 409–452, 1987.
6. Edwards, John W., Applications of Potential Theory to Transonic Aeroelasticity, Paper No. ICAS–86–2.9.1, Presented at the 15th Congress of ICAS, London, England, September 7–12, 1986.
7. Batina John T., Efficient Algorithm for Solution of the Unsteady Transonic Small-Disturbance Equation, *Journal of Aircraft*, vol. 25, no. 7, pp. 598–605, 1988.
8. Vichnevetsky, Robert, and Bowles, John B., *Fourier Analysis of Numerical Approximations of Hyperbolic Equations*, SIAM, Philadelphia, 1982.
9. Vichnevetsky, Robert, Wave Propagation and Reflection in Irregular Grids for Hyperbolic Equations, *Applied Numerical Mathematics*, vol. 3, pp. 133–166, 1987.
10. Trefethen, Lloyd N., Group Velocity in Finite Difference Schemes, *SIAM Review*, vol. 24, no. 2, pp. 113–136, 1982.
11. Anderson, Dale A., Tannehill, John C., and Pletcher, Richard H., *Computational Fluid Mechanics and Heat Transfer*, Hemisphere Publishing Corporation, Washington, 1984.

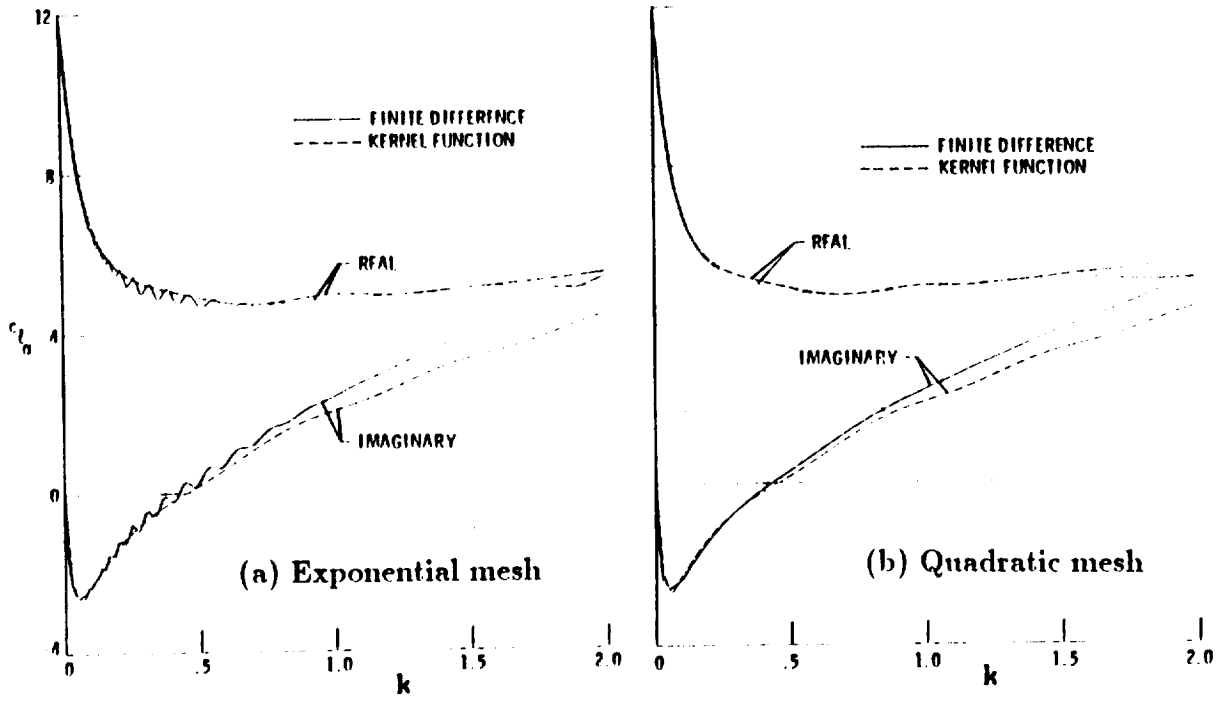

Figure 1.- Unsteady forces calculated using TSD theory at M = 0.85.

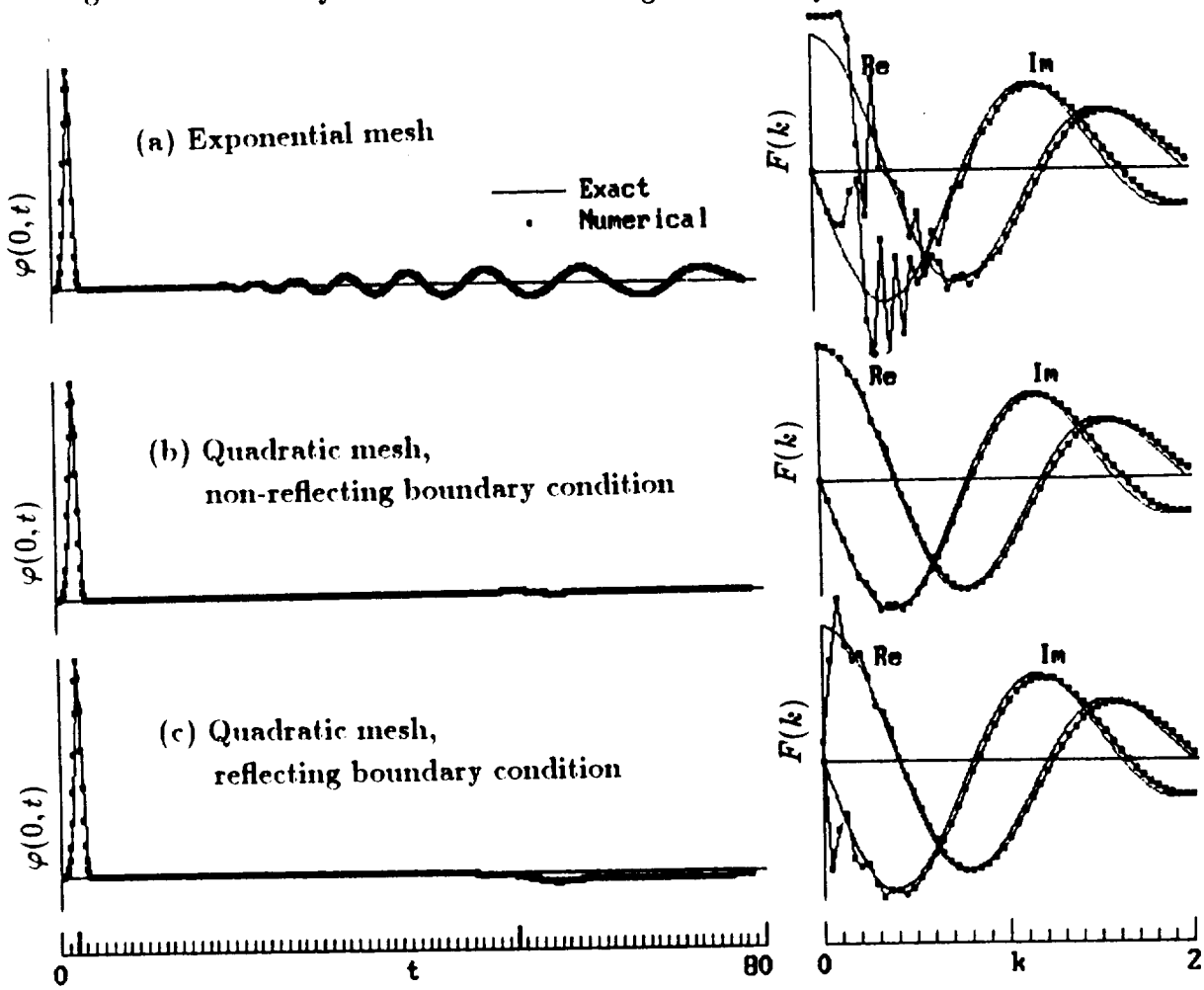

Figure 2.- Time history and frequency response solutions of the one- dimensional model problem using the meshes of the TSD solution in figure 1.

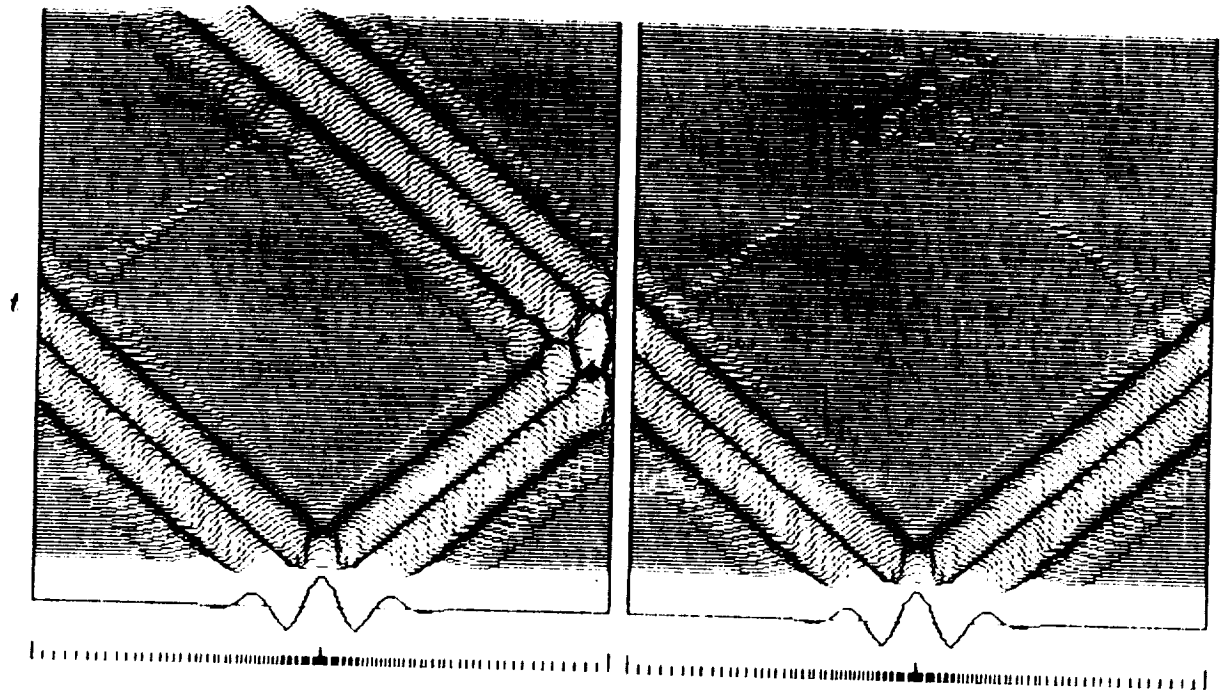

(a) 97 points, reflecting boundary condition

(b) 97 points

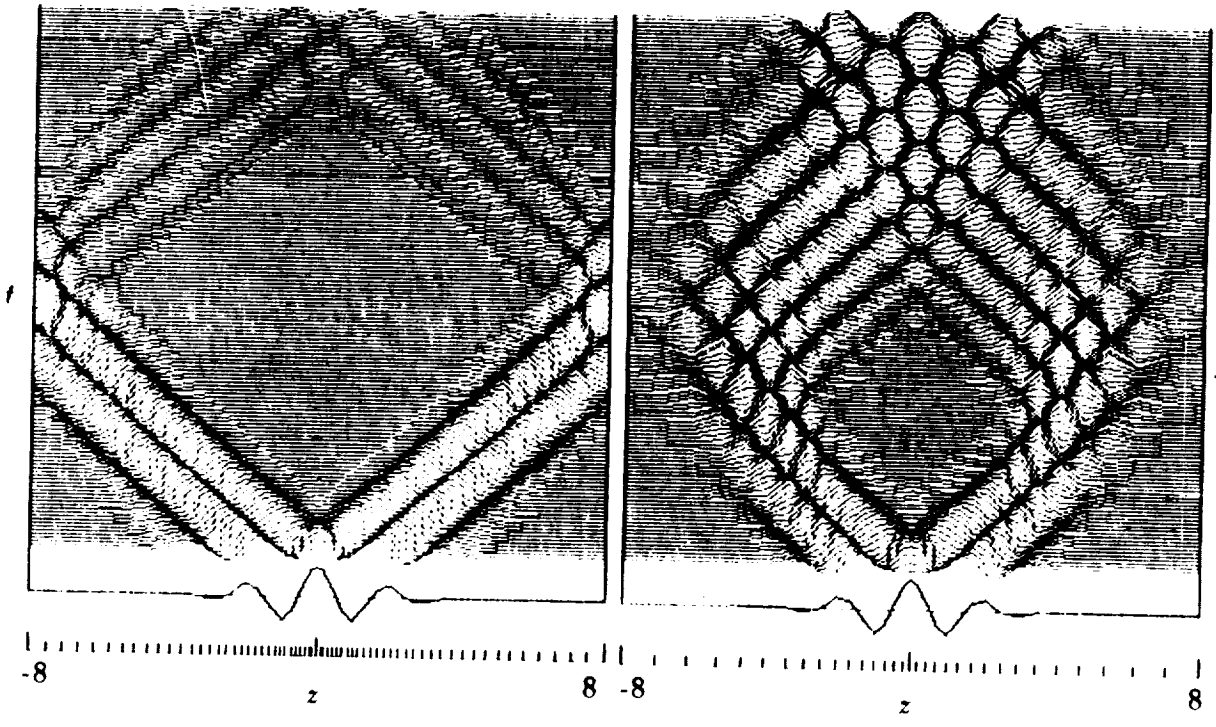

(c) 65 points

(d) 33 points

Figure 3.- Initial value problem on stretched meshes of differing fineness.

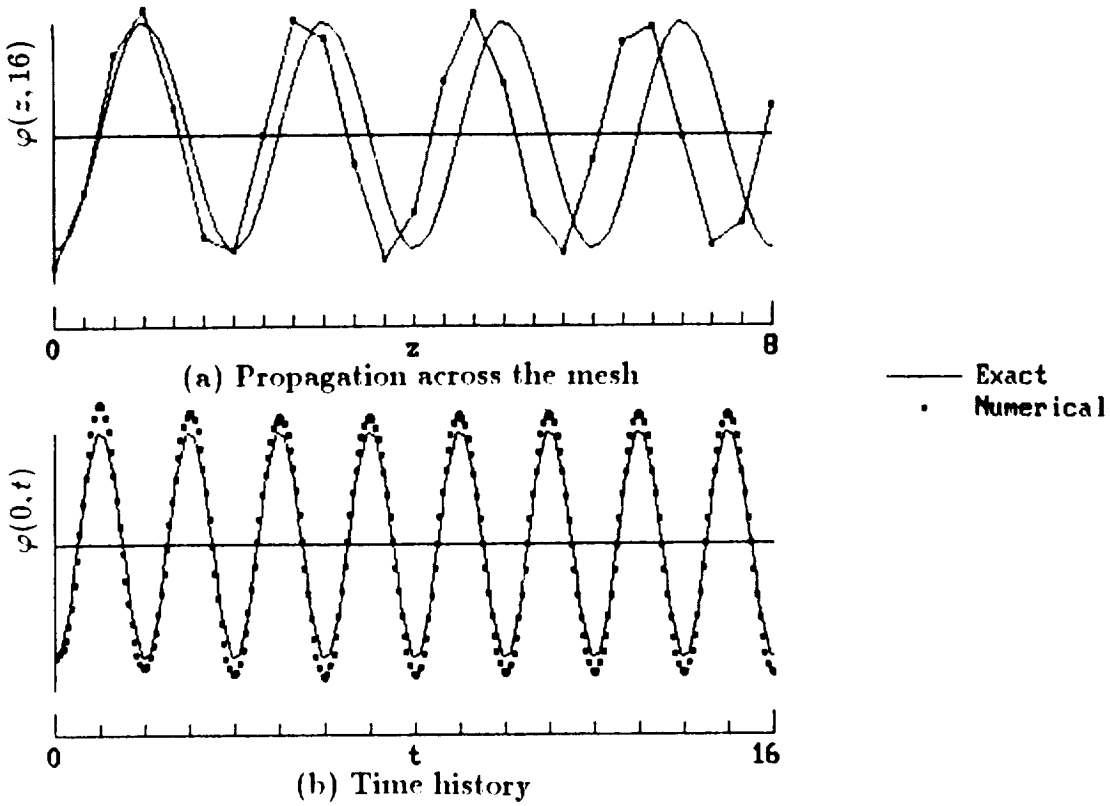

Figure 4.- Comparison of exact and numerical solutions for harmonic boundary condition on uniform mesh; $\omega = \pi$, $h = 1/3$.

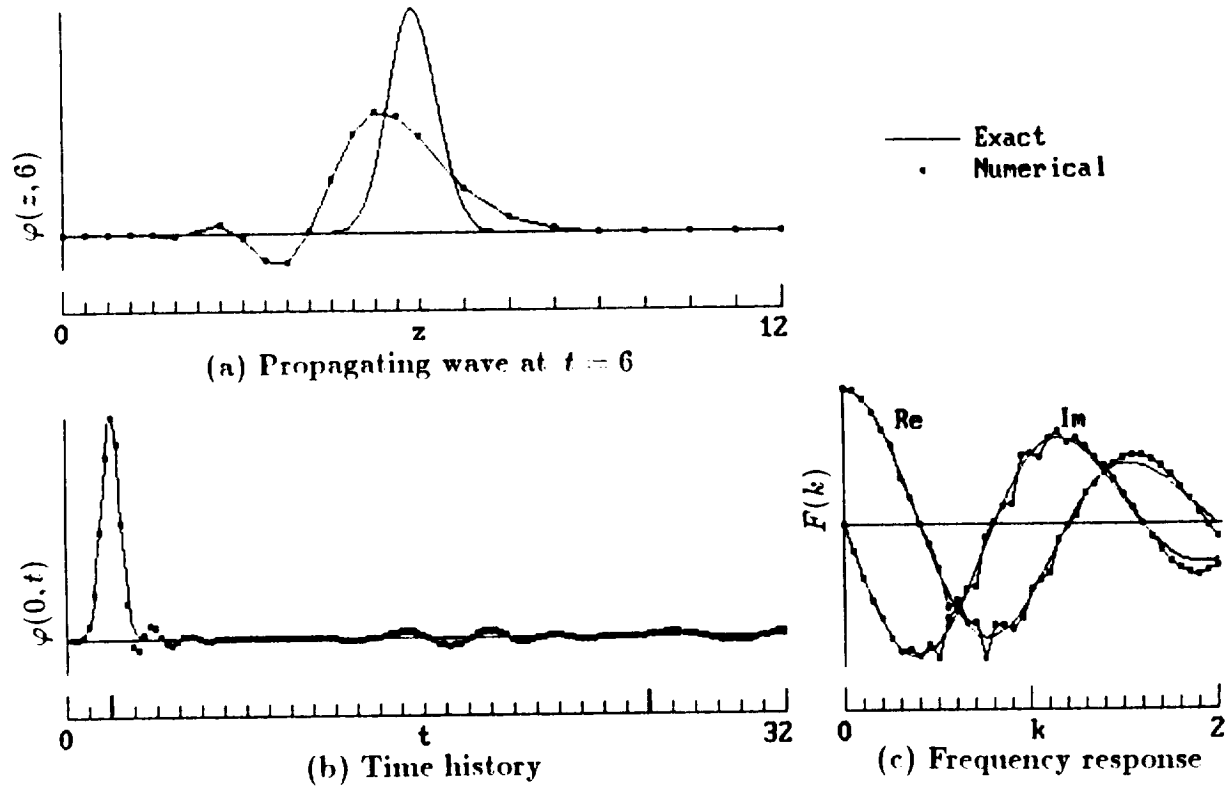

Figure 5.- Comparison of exact and numerical solutions on bi-uniform mesh; $h = 3/8$ and $H = 3/4$.

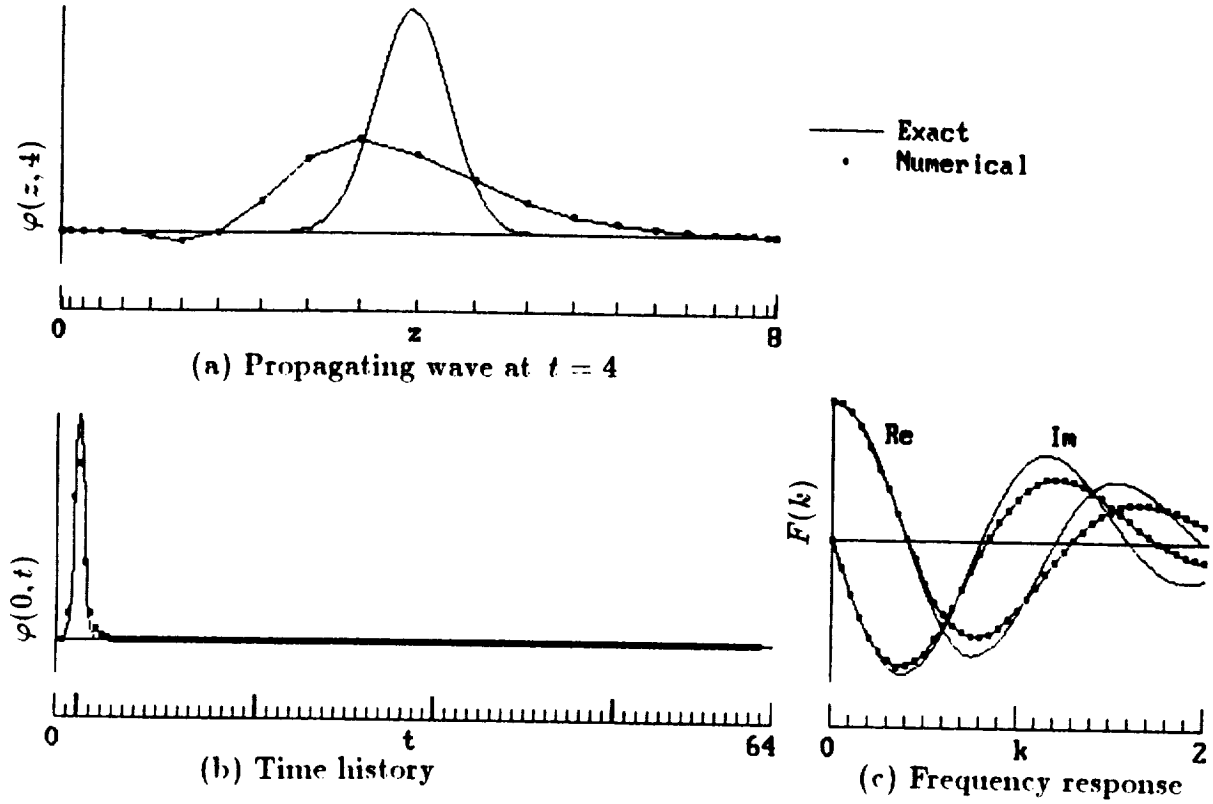

Figure 6.- Comparison of exact and second-order accurate numerical solutions with $\Delta t \approx 1/2$.

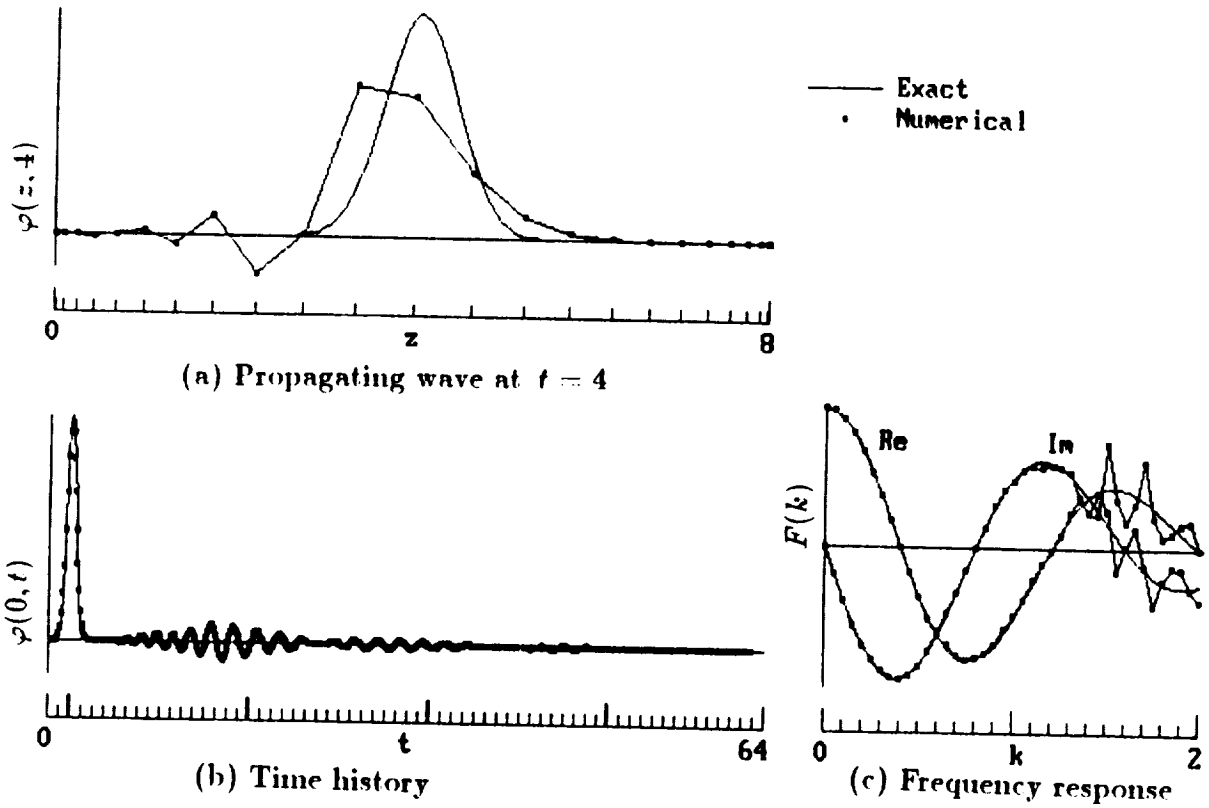

Figure 7.- Comparison of exact and second-order accurate numerical solutions with $\Delta t \approx 1/8$.

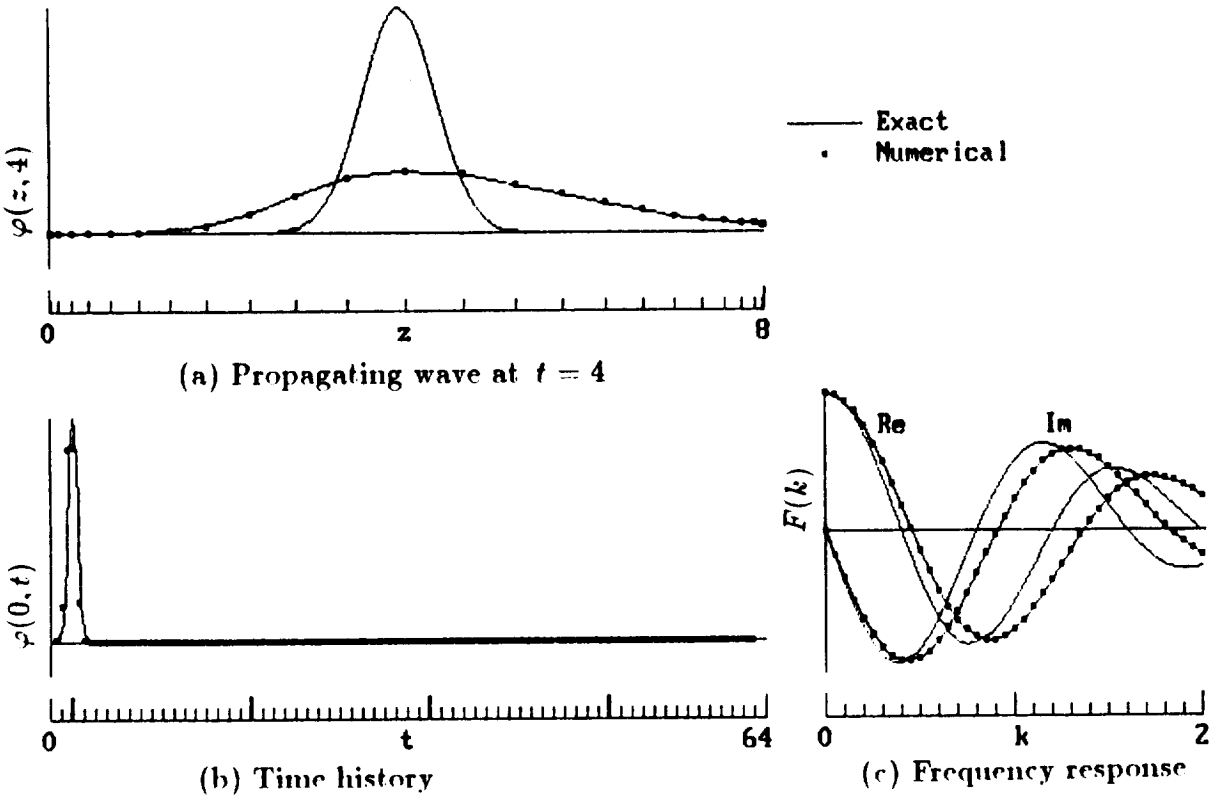

Figure 8.- Comparison of exact and first-order accurate numerical solutions with $\Delta t \approx 1/2$.

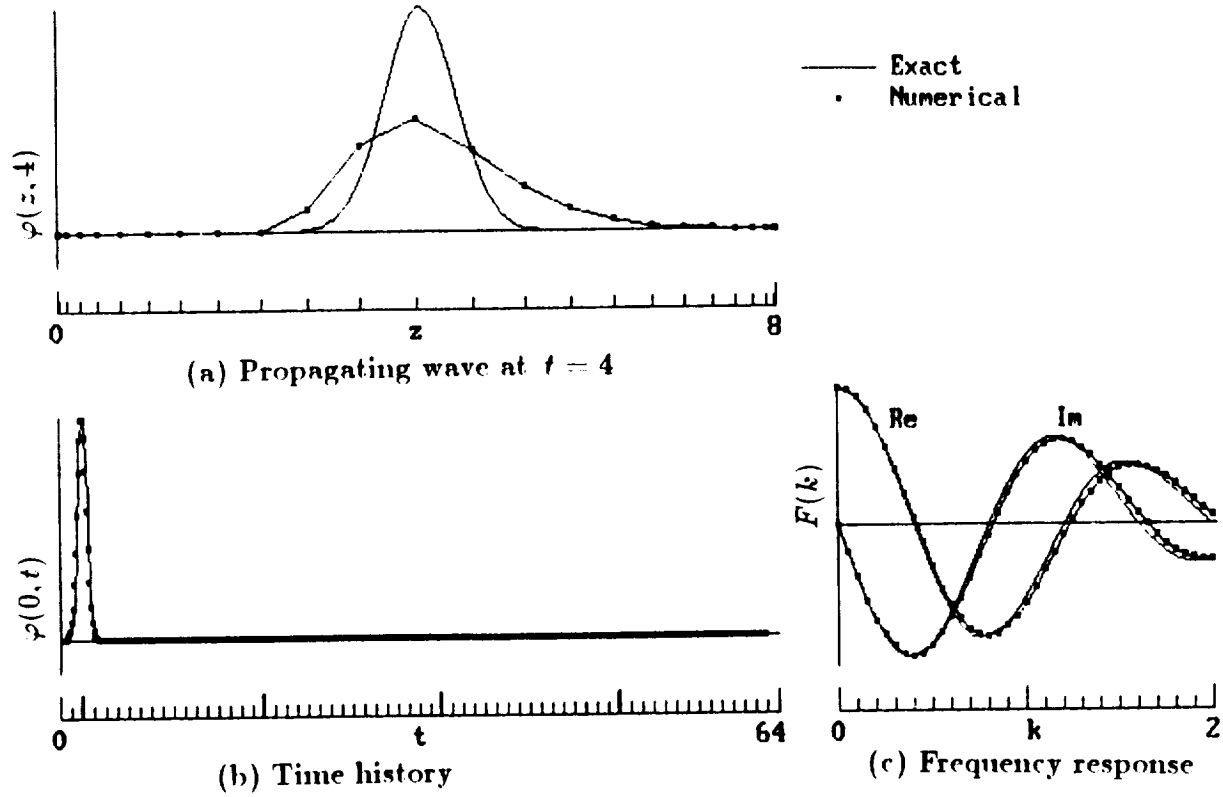

Figure 9.- Comparison of exact and first-order accurate numerical solutions with $\Delta t \approx 1/8$.

NASA National Aeronautics and Space Administration

Report Documentation Page

1. Report No.	2. Government Accession No.	3. Recipient's Catalog No.
NASA TM-102582		

4. Title and Subtitle	5. Report Date
Personal Computer Study of Finite-Difference Methods for the Transonic Small Disturbance Equation	December 1989
	6. Performing Organization Code

7. Author(s)	8. Performing Organization Report No.
Samuel R. Bland	
	10. Work Unit No. 505-63-21

9. Performing Organization Name and Address	11. Contract or Grant No.
NASA Langley Research Center Hampton, Va 23665-5225	
	13. Type of Report and Period Covered
12. Sponsoring Agency Name and Address	Technical Memorandum
National Aeronautics and Space Administration Washington, D.C. 20546-0001	14. Sponsoring Agency Code

15. Supplementary Notes

Presented at Third International Congress of FLuid Mechanics, Cairo, Egypt
January 2-4, 1990

16. Abstract

Calculation of unsteady flow phenomena requires careful attention to the numerical treatment of the governing partial differential equations. The personal computer provides a convenient and useful tool for the development of meshes, algorithms, and boundary conditions needed to provide time accurate solution of these equations. The one-dimensional equation considered in this paper provides a suitable model for the study of wave propagation in the equations of transonic small disturbance potential flow. Numerical results for effects of mesh size, extent, and stretching, time step size, and choice of far-field boundary conditions are presented. Analysis of the discretized model problem supports these numerical results. Guidelines for suitable mesh and time step choices are given.

17. Key Words (Suggested by Author(s))	18. Distribution Statement
Unsteady flow Finite-difference	Unclassified - Unlimited Subject Category 02

19. Security Classif. (of this report)	20. Security Classif. (of this page)	21. No. of pages	22. Price
Unclassified	Unclassified	18	A03